Pion p_T spectra in $p+p$ collisions as a function of $\sqrt{s}$ and event multiplicity

Priyanka Sett[1] and Prashant Shukla[2]
Nuclear Physics Division, Bhabha Atomic Research Center [1,2],
Trombay, Mumbai - 400 085, India
Homi Bhabha National Institute [1,2], Anushaktinagar, Mumbai - 400094, India

arXiv:1408.1034v2 [hep-ph] 3 Sep 2014

Abstract

We study the charged pion transverse momentum (p_T) spectra in p+p collisions as a function of collision energy $\sqrt{s}$ and event multiplicity using Tsallis distribution. This study gives an insight of the pion production process in $p+p$ collisions. The study covers pion spectra measured in $p+p$ collisions at SPS energies (6.27-17.27 GeV), RHIC energies (62.4 GeV and 200 GeV) and LHC energies (900 GeV, 2.76 TeV and 7 TeV). The Tsallis parameters have been obtained and parameterized as a function of $\sqrt{s}$. The study suggests that as we move to higher energy more and more hard processes contribute to the spectra. We also study the charged pion spectra for different event multiplicities in p+p collisions for LHC energies using Tsallis distribution. The variation of the Tsallis parameters as a function of event multiplicity has been obtained and their behavior is found to be independent of collision energy.

1 Introduction

The particle spectra measured in hadronic collisions are of utmost interest because of their fundamental nature and simplicity, which allow to verify pQCD [1, 2] calculations and also help to make comprehensive phenomenological studies. The ratios of the particle yields obtained from the measured spectra allow to get the chemical freeze-out conditions, whereas the spectra themselves reflect the conditions at the kinetic freeze-out. The particle spectra provide useful information about the collision dynamics. The low p_T region of the spectrum corresponds to the particles originating from low momentum transfer and multi-scattering processes (non-perturbative QCD), whereas, the high p_T region comes from the hard-parton-scattering (pQCD) among the initial partons. The transition of this non-perturbative to perturbative dynamics has no sharp boundary, though one can have an estimate from the '$x_T - scaling$' [3]. Extensive [4, 5] and non-extensive [6, 7, 8, 9, 10] statistical approaches have been used to characterize particle spectra in terms of thermodynamic variables. Extensive statistics assume thermal and chemical equilibrium of the system at hadronic phase which lead to an exponential distribution of the particle spectra. In experiments, the particle spectra show a power-law behavior at high p_T. This

[1]email : sett.priyanka@gmail.com
[2]email : pshuklabarc@gmail.com

behavior is reproduced by the non-extensive approach with an additional parameter. In recent times, the Tsallis [6] statistical approach is widely used to describe the particle spectra obtained in high-energy collisions with only two parameters; the temperature T and q, known as non-extensivity parameter which is a measure of temperature fluctuations or degree of non-equilibrium in the system.

The Tsallis distribution gives an excellent description of p_T spectra of all identified mesons measured in $p+p$ collisions at $\sqrt{s} = 200\,\mathrm{GeV}$ [11]. In a recent work [12, 13], the Tsallis distribution has been used to describe the p_T spectra of identified charged hadrons measured in $p+p$ collisions at RHIC and at LHC energies. Such an approach has also been applied to the inclusive charged hadron $p+p$ data in recent publications [14, 15]. It has been shown in Ref. [12, 16] that the functional form of the Tsallis distribution with thermodynamic origin is of the same form as the QCD-inspired Hagedorn formula [17, 18]. This could be the reason of success of Tsallis distribution in $p+p$ collisions which is a power law typical of QCD hard scatterings. The hardness of the spectra is thus related to q and the parameter T governs the contribution from soft collisions.

Using the Tsallis phenomenological function, we review and study the charged pion spectra in $p+p$ collisions in a large energy regime, spanning from SPS [19] (6.27 GeV - 17.27 GeV), RHIC [20] (62.4 and 200 GeV) to LHC [21] (900 GeV, 2.76 TeV and 7 TeV) energies. The object of the present work is to study the behaviour of the Tsallis parameters as a function of collision energy. We also study the charged pion spectra for different event multiplicities in p+p collisions for LHC energies. Among all hadrons, pions are chosen because of their abundance in collisions, simple quark structure and availability of the data at different energies.

2 Formalism

The transverse momentum spectra of hadrons, obtained from different fixed and collider experiments have shown that, the high p_T region of the spectra can be described successfully by the power law,

$$E\frac{d^3N}{dp^3} = C_P p_T^{-n}, \tag{1}$$

where C_P is the normalization constant and n is the power which determines the shape of the spectra at high p_T. However, the low p_T region of the particle spectra shows an exponential shape and can be described by the Boltzmann-Gibbs [22, 23] statistical approach,

$$E\frac{d^3N}{dp^3} = C_B e^{-E/T}, \tag{2}$$

where C_B is the normalization constant, E is the particle energy and T is the temperature of the system.

In the early 80's, Hagedorn [17] proposed a phenomenological function which describes the particle spectra for both the higher and lower p_T regions:

$$E\frac{d^3N}{dp^3} = A\left(1+\frac{p_T}{p_0}\right)^{-n}, \tag{3}$$

where A, p_0 and n are the fit parameters. The above equation describes an exponential behavior for low p_T and a power-law behavior for high p_T.

$$\left(1+\frac{p_T}{p_0}\right)^{-n} \simeq \exp\left(\frac{-np_T}{p_0}\right), \quad \text{for } p_T \to 0 \tag{4}$$

$$\simeq \left(\frac{p_0}{p_T}\right)^{n}, \quad \text{for } p_T \to \infty. \tag{5}$$

The parameter n in this equation is often related to the 'power' in the 'QCD-inspired' quark interchange model [18].

In the late 80's, Tsallis [6] introduced the idea of the non-extensive statistics in place of thermal Boltzmann-Gibbs statistics. This approach includes a parameter q, known as non-extensive parameter which quantifies the temperature fluctuation [24] in the system as : $q-1 = Var(1/T)/\langle T\rangle^2$. The non-extensive statistics assume Boltzmann-Gibbs form in the limit $q \to 1$. In Tsallis approach, the Boltzmann-Gibbs distribution takes the form

$$E\frac{d^3N}{dp^3} = C_q\left(1+(q-1)\frac{E}{T}\right)^{\frac{-1}{q-1}}, \tag{6}$$

where C_q is the normalization factor. One can use the relation $E = m_T$ at mid-rapidity and $n = 1/(q-1)$ in Eq. 6 to obtain :

$$E\frac{d^3N}{dp^3} = C_n\left(1+\frac{m_T}{nT}\right)^{-n}, \tag{7}$$

where, C_n is the normalization factor. Eq. 7 can be re-written as :

$$\frac{1}{2\pi p_T}\frac{d^2N}{dp_T dy} = C_n\left(1+\frac{m_T}{nT}\right)^{-n}, \tag{8}$$

The value of C_n can be obtained by integrating Eq. 8 over momentum space :

$$C_n = \frac{dN/dy}{\int_0^\infty \left(1+\frac{m_T}{nT}\right)^{-n} 2\pi p_T dp_T}, \tag{9}$$

Here the quantity dN/dy is the p_T integrated yield. Eq. 7 with the normalization constant takes the form [11] :

$$E\frac{d^3N}{dp^3} = \frac{1}{2\pi}\frac{dN}{dy}\frac{(n-1)(n-2)}{(nT+m(n-1))(nT+m)}\left(\frac{nT+m_T}{nT+m}\right)^{-n}, \tag{10}$$

Table 1: The center of mass energy and rapidity of the data used for the study.

Experiments	Center of mass energy (GeV)	Rapidity	Particles Studied
SPS	6.27, 7.74, 8.76, 12.32, 17.27	0.0–0.2	π^-
RHIC	62.4, 200	$\|y\| < 0.35$	π^+, π^-
LHC	900, 2760, 700	$\|y\| < 1.0$	π^+, π^-

Larger values of q correspond to smaller values of n which imply dominant hard QCD point-like scattering. Both n and q have been interchangeably used in Tsallis distribution [7, 11, 20, 25, 26]. The Tsallis interpretation of parameters T as temperature and q as non-extensivity parameter is more suited for heavy ion collisions while for $p+p$ collisions Hagedorn interpretation in terms of power n and a parameter $T = p_0/n$ which controls soft physics processes is more meaningful. Phenomenological studies suggest that, for quark-quark point scattering, $n \sim 4$ [27, 28] and when multiple scattering centers are involved n grows larger.

There are many other forms of Eq. 10, which are used often to describe particle spectra in literature, see e.g. Refs. [7, 20, 25, 26, 29, 30, 31].

3 Results and Discussions

All the studies are performed with Eq. 10 and the fit parameters n, T and dN/dy are obtained. The different experiments, energies, rapidity ranges and particles used in the analysis are summarized in Table 1. For SPS energies only available data is for π^- measured by NA61 Collaboration [19], for RHIC and LHC energies we use $(\pi^+ + \pi^-)/2$. All the data used are measured in mid-rapidity and are given for unit rapidity. The difference in rapidity range is not expected to affect the behaviour of the spectra. CMS experiment presented [21] transverse momentum spectra for different events classified on the basis of number of true tracks referred here as track multiplicity of event or simply multiplicity. Each multiplicity class is represented by average number of tracks ($\langle N_{tracks} \rangle$).

3.1 Tsallis parameters as a function of $\sqrt{s}$ in $p+p$ system :

In this analysis all the Tsallis parameters are obtained for charged pion spectra as a function of $\sqrt{s}$ in $p+p$ system for SPS [19], RHIC [20] and LHC [21] energies. Similar study is available in Ref. [12] using RHIC and LHC data and in Ref. [13] for SPS and LHC data.

The pion p_T spectra measured in $p+p$ collisions at different $\sqrt{s}$ are shown in Fig. 1

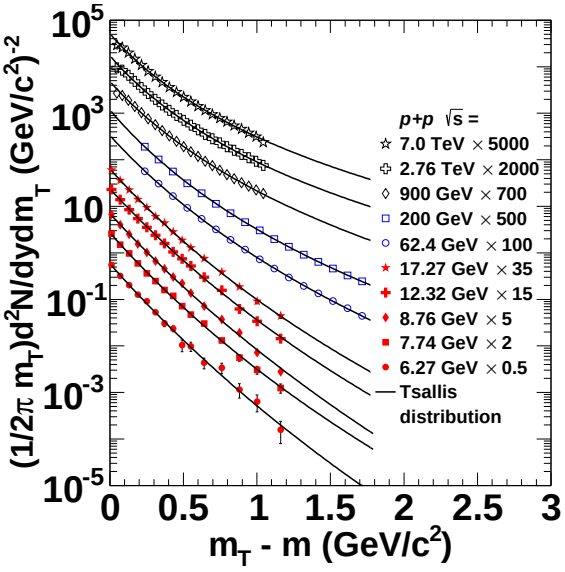

Figure 1: (Color online) The invariant yield spectra of charged pions as a function of $(m_T - m)$ for SPS [19] energies 6.27 GeV, 7.74 GeV, 8.76 GeV, 12.32 GeV and 17.27 GeV, RHIC [20] energies 62.4 GeV and 200 GeV and LHC [21] energies 900 GeV, 2.76 TeV and 7 TeV. The solid lines are the Tsallis function (Eq. 10). The negative pion yields are plotted for SPS energies and for all other energies, average yield for positive and negative pion are plotted.

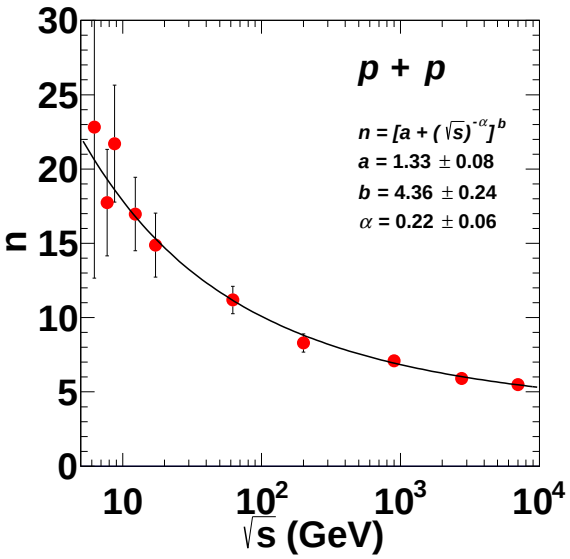

Figure 2: (Color online) The variation of the Tsallis parameter n for charged pions as a function of $\sqrt{s}$. The solid curve represents the parameterization $(a + (\sqrt{s})^{-\alpha})^b$.

Table 2: Values of the χ^2/NDF for Tsallis fits of pion spectra at different $\sqrt{s}$.

$\sqrt{s}$	χ^2/NDF
6.27 GeV	6.31/12
7.74 GeV	5.80/12
8.76 GeV	10.68/12
12.32 GeV	9.25/12
17.27 GeV	2.65/12
62 GeV	0.74/11
200 GeV	0.48/11
900 GeV	24.33/19
2.76 TeV	5.59/19
7.00 TeV	13.11/19

along with with Tsallis fits (Eq. 10) shown by solid lines. The spectra are scaled by arbitrary factors (given in figure) for visual clarity. In case of RHIC data, we restrict the p_T range to 1.7 GeV/c^2 to have similar p_T range at all energies. It can be noticed that the spectra become harder with increase in $\sqrt{s}$ which is depictive of occurrence of harder scatterings at higher collision energy. The χ^2 per degree of freedom χ^2/NDF values for all the fits are given in Table 2. The χ^2/NDF values are $\lesssim 1$, which is indicative of good fit quality.

The parameters n and T obtained from this analysis are shown in Fig. 2 and Fig. 3, respectively, as a function of $\sqrt{s}$. The variation of dN/dy as a function of $\sqrt{s}$ is shown in Fig. 4. The parameter n decreases with increasing $\sqrt{s}$ and starts saturating at LHC energies. The value of T also reduces slowly from SPS energies to LHC energies. The integrated yield dN/dy increases 10 times when going from SPS to highest LHC energy.

Larger value of n (also larger value of T) suggests that the spectra has contribution from processes involving small momentum transfer arising due to the re-scattering, re-combination of partons, fragmentation from strings etc. Whereas, smaller values of n are indicative of harder processes are involved in particle-production. Thus the spectra at SPS energies have large softer contribution and as the collision energy increases more and more contribution from hard processes are added.

All the three parameters can be parametrized by a function of type

$$f(\sqrt{s}) = \left(a + (\sqrt{s})^{-\alpha}\right)^b \tag{11}$$

Here $a = 1.33 \pm 0.08$, $\alpha = 0.22 \pm 0.06$ and $b = 4.36 \pm 0.24$ for $n(\sqrt{s})$, $a = 2.63 \pm 0.62$, $\alpha = 0.04 \pm 0.02$ and $b = 3.76 \pm 0.49$ for $T(\sqrt{s})$ and $a = 0.65 \pm 0.01$, $\alpha = 0.22 \pm 0.01$ and $b = -4.78 \pm 0.03$ for $dN(\sqrt{s})/dy$. Using the parameterizations for n by Eq. 11 we get $n \sim 3.46$ in the limit $\sqrt{s} \to \infty$. The extrapolated values for n, T and dN/dy for $\sqrt{s} = 14$ TeV are, $n \sim 5.09$, $T \sim 90.33$ MeV and $dN/dy \sim 3.44$.

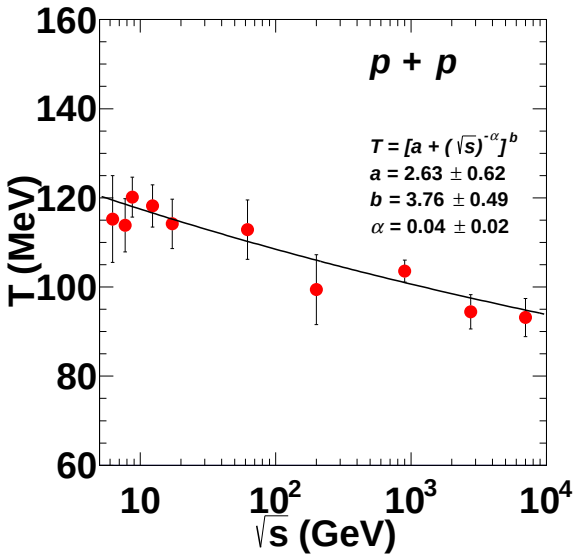

Figure 3: (Color online) The variation of the Tsallis parameter T for charged pions as a function of $\sqrt{s}$. The solid curve represents the parameterization $(a + (\sqrt{s})^{-\alpha})^b$.

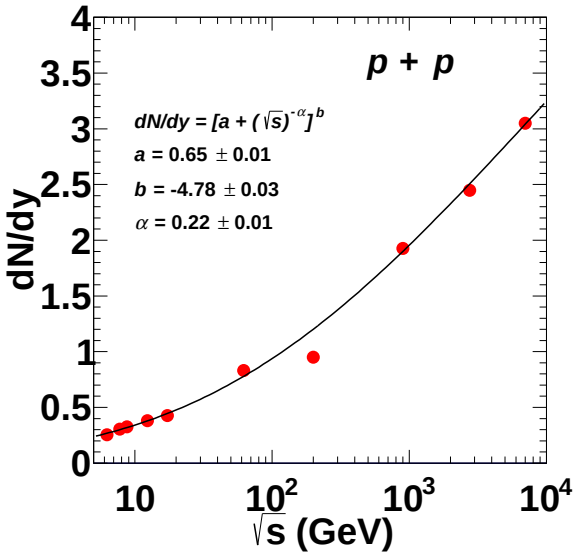

Figure 4: (Color online) The variation of the integrated yield dN/dy for charged pions as a function of $\sqrt{s}$. The solid curve represents the parameterization $(a + (\sqrt{s})^{-\alpha})^b$.

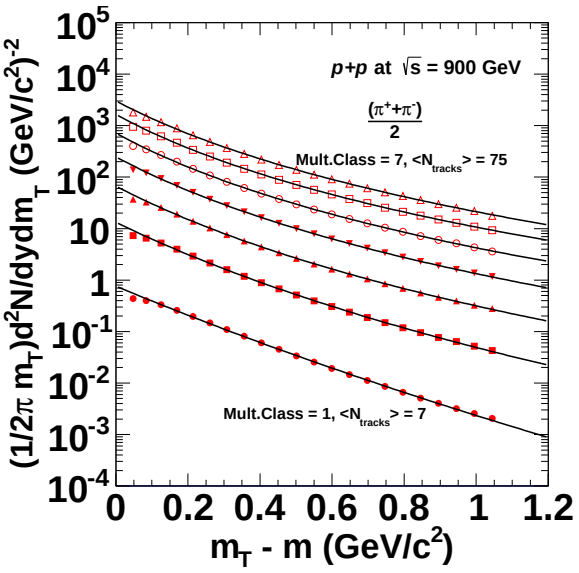

Figure 5: (Color online) The invariant yield spectra of $(\pi^+ + \pi^-)/2$ [21], as a function of $m_T - m$ for $p + p$ collisions at $\sqrt{s} = 900$ GeV. The yields are shown for $\langle N_{tracks} \rangle$ 7, 16, 28, 40, 52, 63 and 75. The spectra are scaled up for clarity by a factor of 6^i, where i = 0, 1, 2, 3, 4, 5 and 6. The solid lines show the Tsallis fits.

3.2 Tsallis parameters as a function of multiplicity ($\langle N_{tracks} \rangle$) for LHC energies :

The Tsallis parameters for charged pion spectra are studied as a function of event multiplicity for different LHC energies 900 GeV, 2.76 and 7 TeV. The event multiplicity data was also studied in a recent work [10] but our analysis and interpretations are different.

The invariant yield spectra corresponding to different multiplicities are fitted with Eq. 10, are shown by the solid black lines in Fig. 5 for 900 GeV, in Fig. 6 for 2.76 TeV and in Fig. 7 for 7 TeV center of mass energy. The spectra are scaled up for distinctness. The Tsallis distribution describes all the spectra well, shown by the χ^2/NDF values given in Table 3. The χ^2/NDF values are little higher for some of the lower multiplicities due to the deviation of first data point in p_T spectra with the curve.

The parameters n and T obtained from the fits are shown in Fig. 8 and Fig. 9 respectively, as a function of $\langle N_{tracks} \rangle$. The circles, squares and triangles correspond to the parameter values obtained from data at 900 GeV, 2.76 TeV and 7 TeV, respectively. It is seen that both the parameters n and T decrease rapidly and then start saturating with the increase of $\langle N_{tracks} \rangle$ for all three energies. This variation (of n and T) is very similar to the variation which we find as a function of $\sqrt{s}$. It means that events with higher multiplicity have larger contribution from hard processes. The value of n for high multiplicity events at 7 TeV is ~ 4 which is depictive of production from point quark-quark

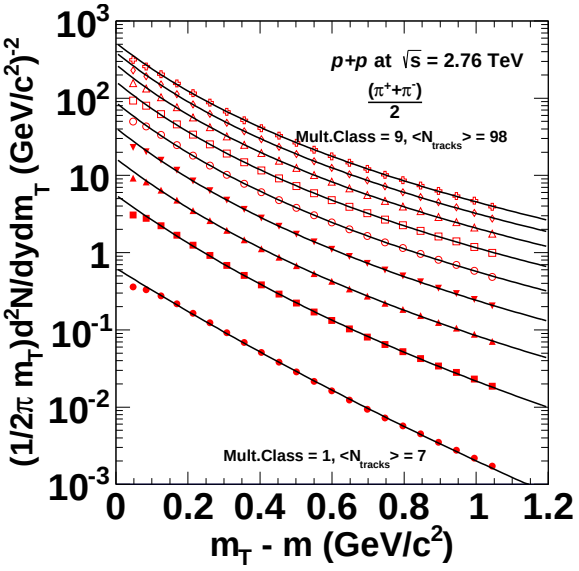

Figure 6: (Color online) The invariant yield spectra of $(\pi^+ + \pi^-)/2$ [21], as a function of $m_T - m$ for $p + p$ collisions at $\sqrt{s} = 2.76$ TeV. The yields are shown for $\langle N_{tracks} \rangle$ 7, 16, 28, 40, 52, 63, 75, 86 and 98. The spectra are scaled up for clarity by a factor of 3^i, where i = 0, 1, 2, 3, 4, 5, 6, 7 and 8. The solid lines show the Tsallis fits.

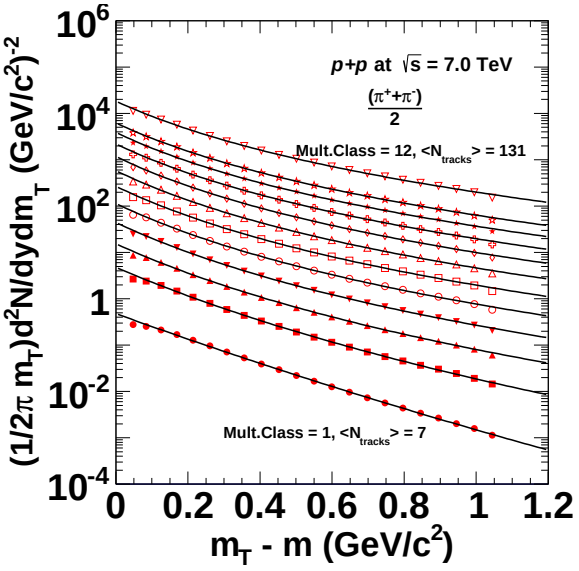

Figure 7: (Color online) The invariant yield spectra of $(\pi^+ + \pi^-)/2$ [21], as a function of $m_T - m$ for $p + p$ collisions at $\sqrt{s} = 7.00$ TeV. The yields are shown for $\langle N_{tracks} \rangle$ 7, 16, 28, 40, 52, 63, 75, 86, 98, 109, 120 and 131. The spectra are scaled up for clarity by a factor of 3^i, where i = 0, 1, 2, 3, 4, 5, 6, 7, 8, 9, 10 and 11. The solid lines show the Tsallis fits.

Table 3: Values of the χ^2/NDF for the Tsallis fits in different event multiplicities.

$\langle N_{tracks} \rangle$	χ^2/NDF values for		
	900 GeV	2.76 TeV	7.0 TeV
7	48.89/18	57.66/18	48.10/18
16	25.21/18	26.38/18	27.76/18
28	9.97/18	11.47/18	22.83/18
40	7.20/18	6.91/18	19.25/18
52	8.00/18	6.08/18	22.52/18
63	9.18/18	6.44/18	26.30/18
75	15.01/18	9.05/18	21.30/18
86		8.16/18	19.24/18
98		11.91/18	23.59/18
109			20.82/18
120			16.85/18
131			19.77/18

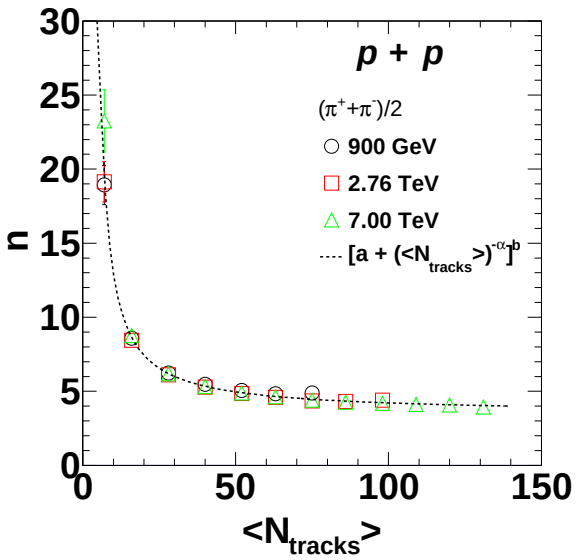

Figure 8: (Color online) The variation of the Tsallis parameter n for charged pions as a function of $\langle N_{tracks} \rangle$. The variation is shown for 900 GeV by black circles, 2.76 TeV by red squares and 7.00 TeV by green triangles. The dashed curve represents the parameterization $(a + (\langle N_{tracks} \rangle)^{-\alpha})^b$.

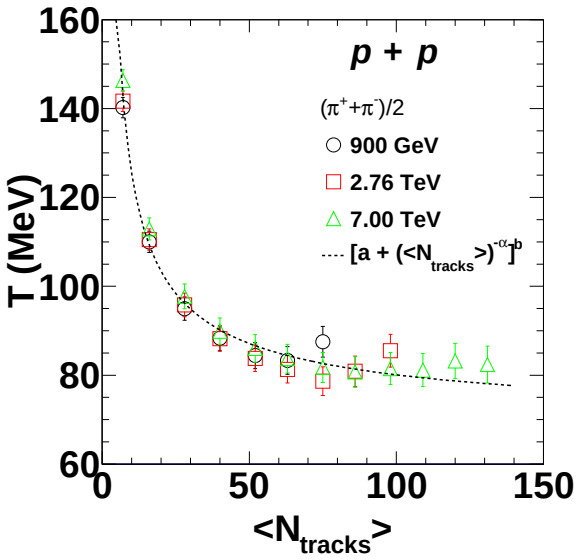

Figure 9: (Color online) The variation of the Tsallis parameter T for charged pions as a function of $\langle N_{tracks} \rangle$. The variation is shown for 900 GeV by black circles, 2.76 TeV by red squares and 7.00 TeV by green triangles. The dashed curve represents the parameterization $(a + (\langle N_{tracks} \rangle)^{-\alpha})^{b}$.

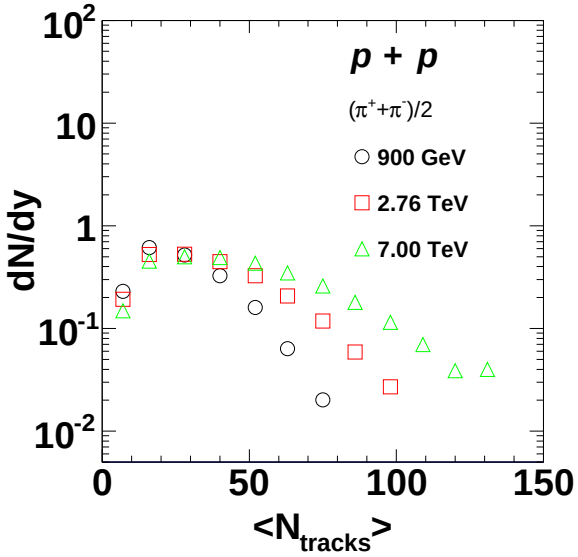

Figure 10: (Color online) The variation of the integrated yield dN/dy for charged pions as a function of $\langle N_{tracks} \rangle$. The variation is shown for 900 GeV by black circles, 2.76 TeV by red squares and 7.00 TeV by green triangles.

scattering. The variation of n and T as a function of $\langle N_{tracks} \rangle$ can be described by the same curve given in the figure for all three energies and are parameterized by,

$$f((< N_{tracks} >) = \left(a + (< N_{tracks} >)^{-\alpha}\right)^{b} \tag{12}$$

Here $a = 1.13 \pm 0.01$, $\alpha = 0.81 \pm 0.04$ and $b = 10.32 \pm 0.76$ for $n(\langle N_{tracks} \rangle)$ and $a = 2.20 \pm 0.06$, $\alpha = 0.56 \pm 0.08$ and $b = 5.33 \pm 0.23$ for $T(\langle N_{tracks} \rangle)$.

The p_T integrated pion yield distribution in different multiplicity classes is shown in Fig. 10 for the three LHC energies. The total p_T integrated pion yield for each energy can be obtained by integrating the above distributions over all multiplicity classes. It is noticed that as the energy increases more and more high mutliplicity events are added in the sample with mean of the distribution shifting towards higher $\langle N_{tracks} \rangle$.

4 Conclusion

This work presented the study of the transverse momentum spectra of the charged pions for different collisional energies and also for different event-multiplicities (at LHC energies) using Tsallis distribution. The Tsallis parameter n decreases with increasing $\sqrt{s}$ and starts saturating at LHC energies. The value of T also reduces slowly from SPS energies to LHC energies. It means that the spectra at SPS energies have large softer contribution and as the collision energy increases more and more contribution from hard processes are added. The p_T integrated pion yield increases with increasing $\sqrt{s}$ and becomes 10 times when going from SPS to highest LHC energy. The Tsallis parameters are also obtained as a function of event multiplicity for all three LHC energies which can be described by the same curve. The variation of n and T as a function of multiplicity is very similar to the variation which we find as a function of $\sqrt{s}$. It means that events with higher multiplicity have larger contribution from hard processes. The value of n for high multiplicity events at 7 TeV is ~ 4 which is depictive of production from point quark-quark scattering. The p_T integrated pion yield distribution for the three LHC energies shows that as the energy increases, more and more high mutliplicity events are added in the sample with mean of the distribution shifting towards higher multiplicity.

References

[1] G. Sterman *et al.* (CTEQ Collaboration), Rev. Mod. Phys. **67**, 157 (1995).

[2] J.F. Owens *et al.*, Phys. Rev. D**18**, 1501 (1978).

[3] R. Blankenbecler, S.J. Brodsky and J.F. Gunion, Phys. Lett. B**42**, 461 (1972).

[4] E. Fermi, Progress Theor. Phys., **5**, 570 (1950).

[5] A. Andronic, P. Braun-Munzinger, J. Stachel, Nucl. Phys. A**772**, 167 (2006).

[6] C. Tsallis, J. Stat. Phys. **52**, 479 (1988).

[7] T.S. Biro, G. Purcsel and K. Urmossy, Eur. Phys. J. A**40**, 325 (2009).

[8] W.M. Alberico and A. Lavagno, Eur. Phys. J. A**40**, 313 (2009).

[9] T.S. Biro and G. Purcsel, Phys. Rev. Lett. **95**, 162302 (2005).

[10] K. Urmossy, arXiv:1212.0260[hep-ph].

[11] A. Adare *et al.* (PHENIX Collaboration), Phys.Rev. D**83**, 052004 (2011).

[12] P.K. Khandai, P. Sett, P. Shukla and V. Singh, Int. J. Mod. Phys. **28**, 1350066 (2013).

[13] M. Rybczynski and Z. Wlodarczyk, Eur. Phys. J. C**74**, 2785 (2014).

[14] M.D. Azmi and J. Cleymans, J. Phys. G**41**, 065001 (2014).

[15] J. Cleymans *et al.*, Phys. Lett. B**723**, 351 (2013).

[16] C.Y. Wong and G. Wilk, Phys. Rev. D**87**, 114007 (2013).

[17] R. Hagedorn, Riv. del Nuovo Cim. **6N 10**, 1 (1984).

[18] R. Blankenbecler and S. J. Brodsky, Phys. Rev. D**10**, 2973 (1974).

[19] N. Abgrall *et al.* Eur. Phys. C**74**, 2794 (2014).

[20] A. Adare *et al.* (PHENIX Collaboration), Phys. Rev. C**83**, 064903 (2011).

[21] S. Chatrchyan *et al.* (CMS Collaboration), Eur. Phys. J. C**72**, 2164 (2012).

[22] R. Hagedorn, Nuovo Cim. Suppl. **3**, 147 (1965).

[23] D.B. Walton and J. Rafelski, Phys. Rev. Lett. **84**, 31 (2000).

[24] G. Wilk and Z. Wlodarczyk, Phys. Rev. Lett. **84**, 2770 (2000).

[25] B.I. Abelev *et al.* (STAR Collaboration), Phys. Rev. C**75**, 64901 (2007).

[26] J. Cleymans and D. Worku, Eur. Phys. J. A**48**, 160 (2012).

[27] R. Blankenbecler, S.J. Brodsky and J. Gunion, Phys. Rev. D**12**, 3469 (1975) .

[28] S.J. Brodsky, H.J. Pirner and J. Raufeisen, Phys. Lett. B**637**, 58 (2006).

[29] T.S. Biro, K. Urmossy and G.G. Barnafoldi, J. Phys. G**35**, 044012 (2008).

[30] K. Aamodt *et al.* (ALICE Collaboration), Eur. Phys. J. C**71**, 1655 (2011).

[31] J. Adams *et al.* (STAR Collaboration), Phys. Lett. B**637**, 161 (2006).